Astron. Astrophys. 334, 314–324 (1998)

ASTRONOMY AND ASTROPHYSICS

New features in type IV solar radio emission: combined effects of plasma wave resonances and MHD waves

G.P. Chernov[1], **A.K. Markeev**[1], **M. Poquérusse**[2], **J.L. Bougeret**[2], **K.-L. Klein**[3], **G. Mann**[4], **H. Aurass**[4], **and M.J. Aschwanden**[5]

[1] 142092 IZMIRAN, Troitsk, Moscow Region, Russia
[2] DESPA, URA CNRS 264, Observatoire de Paris, F-92195 Meudon Cedex, France
[3] DASOP, URA CNRS 2080, Observatoire de Paris, F-92195 Meudon Cedex, France
[4] Astrophysikalisches Institut Potsdam, Observatorium für solare Radioastronomie, An der Sternwarte 16, D-14482 Potsdam, Germany
[5] University of Maryland, Astronomy Department, College Park, MD 20742, USA

Received 4 August 1997 / Accepted 4 December 1997

Abstract. An intense and complex type IV solar radio burst over the time period 1992 0217 08–12 was recorded simultaneously by 3 spectrographs, *ARTEMIS* (100–500 MHz), *OSRA* (200–400 MHz) and *IZMIRAN* (180–270 MHz), and by the Nançay radioheliograph. For $\approx$ 2 hours, the event exhibited strong pulsations on various time scales and "zebra patterns" with new features: sudden frequency shifts of the whole pattern, splitting of individual zebra stripes into two stripes, structuration of the upper-frequency split stripes into emission dots in phase with $\approx$ 0.2 s pulsations. Another new and spectacular feature was a $\approx$ 10 MHz bandwidth emission at the high frequency cut-off of the whole event, oscillating between 350 and 450 MHz in phase with $\approx$ 3 min pulsations, and itself structured by the $\approx$ 0.2 s pulsations.

Another property observed for the first time was that the circular polarization of zebra patterns changed sign during the event, possibly due to magnetic field reversal at some point of a long-lasting magnetic reconnection process in the upper corona. According to a classical picture, electrons are accelerated in the current sheet and trapped in the magnetic arch. Pulsations are due to MHD waves affecting the whole arch and electron beams as well.

We confront two existing theories to these new observational features. The $l + w \Rightarrow t$ model (Chernov 1976, 1989), based on Langmuir wave – whistler coupling at normal and anomalous Doppler resonance, can account for all the observed fine structures of zebra patterns, and gives a plausible magnetic field of 11×10^{-4}T in the source. The Winglee & Dulk (1986) model, based on electron–cyclotron maser emission of upper-hybrid waves at double plasma resonance, seems the most adequate to account for the evolving emission line, with its source in the dense current sheet.

Key words: plasmas – radiation mechanisms: non-thermal – Sun: activity – Sun: corona – Sun: magnetic fields – Sun: radio radiation

Send offprint requests to: Michel.Poquerusse@obspm.fr

1. Introduction

Long-lasting metric continuum radiation, like noise storms and certain species of type IV bursts, are signatures of coronal particle acceleration which often occurs without conspicuous Hα or microwave signatures in the underlying atmosphere. These events allow us to investigate how plasma–magnetic field interactions in the solar corona can produce suprathermal electron populations over periods from tens of minutes to several hours, and how wave-particle and wave-wave interactions lead to characteristic fine structures of the emission. As these processes depend on the characteristic frequencies of the coronal plasma, such fine structures may eventually also provide a measurement of coronal electron densities and magnetic field strengths.

An intense and complex type IV event of this category (weak Hα and microwave activity) was observed in great detail on 1992 0217 by 3 different radiospectrographs at decimetric and metric wavelengths:

1. *ARTEMIS* (Meudon, France) – digital recording in the range 100–500 MHz and time resolution of 0.01 s (Maroulis et al. 1993);
2. *OSRA* (Tremsdorf near Potsdam, Germany) – analog recording in the range 40–800 MHz (Mann et al. 1992);
3. *IZMIRAN* (Moscow, Russia) – analog recording in the range 180–270 MHz, with high frequency and time resolutions (0.2 MHz, 0.02 s) in the domain 228–264 MHz (Chernov, Korolev, & Markeev 1975); plus some fixed-frequency radiometers, including a 10-cm receiver.

The source position and polarization were measured with the *Nançay radioheliograph (NRH)* at frequencies of 164, 237, 327, and 407 MHz, with a time resolution of 1 s (Radioheliograph group 1989).

The event produced a wealth of fine structures for more than 2 hours. The main features were recorded independently by all 3 spectrographs, demonstrating their solar origin. In addition to the features frequently observed in type IV bursts (pulsations and "zebra patterns"), the event exhibited unprecedented features: *IZMIRAN* spectrograph discovered new sub-structures of

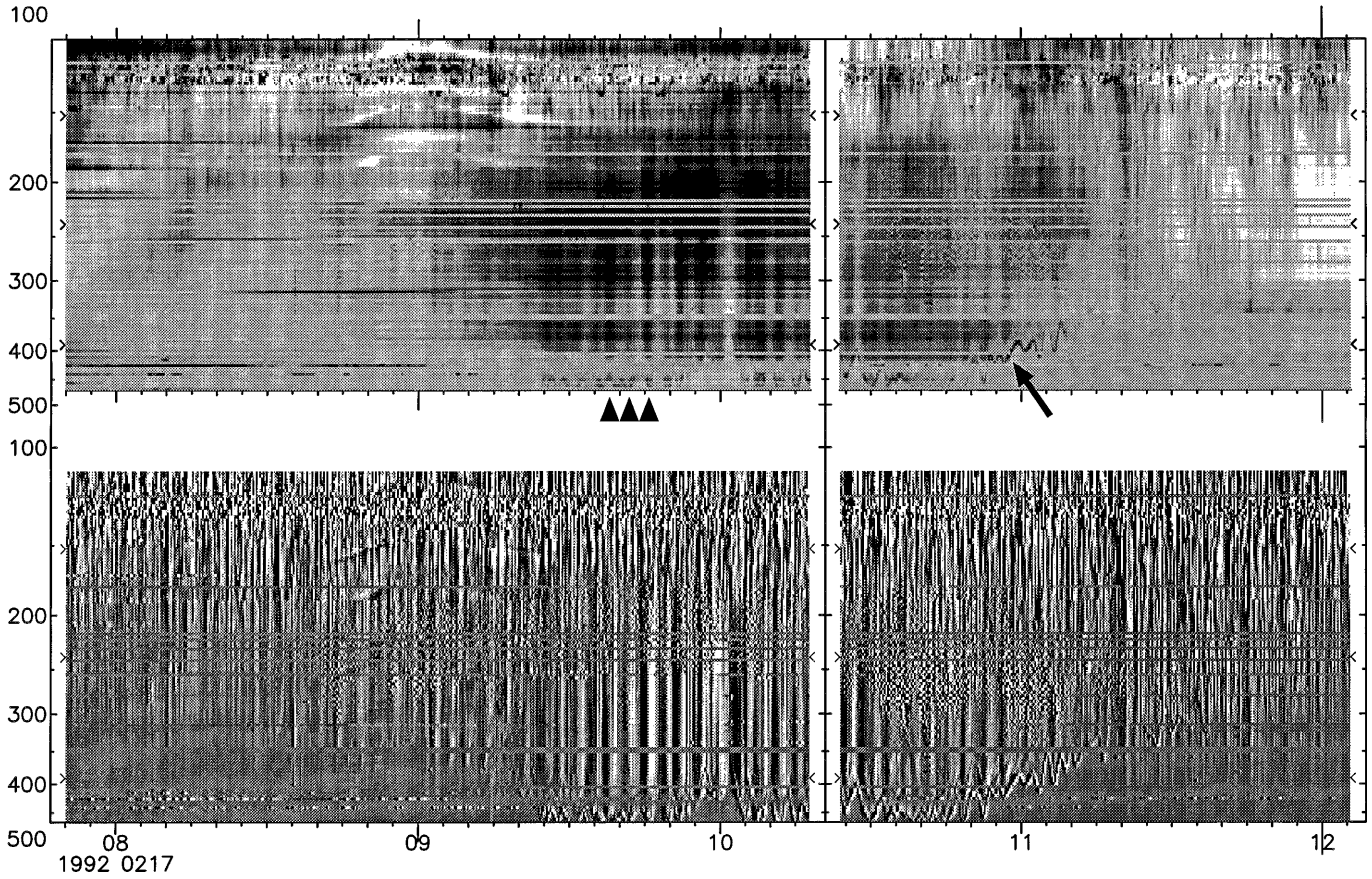

Fig. 1. *ARTEMIS* dynamic spectrum in its full 100–500 MHz frequency range, over the 4 hours of the event ("smoothed data"). Top: flux density; bottom: time derivative. The most prominent structures are broadband 3-min pulsations, with a high-frequency cutoff at ≈ 400 MHz, oscillating in frequency and synchronized with the "evolving emission line" (EEL). The triangles point to three particular maxima of the pulsations; the arrow points to an intense phase of the EEL. The "moiré" structure (at 200–250 MHz before 10 UT and 250–300 MHz after), is produced by the filtering effect of ARTEMIS discontinuous frequency coverage on zebra patterns.

zebra patterns, and *ARTEMIS* spectrograph discovered a long-lasting "evolving emission line". These peculiar features, which seem to be hidden in other large events, challenge our understanding of physical mechanisms that operate in type IV radio sources.

In Sect. 2, we will describe the event, with emphasis on the features never seen before. In Sect. 3, we will compare how well the two leading theories of zebra patterns can explain the new features. In Sect. 4, we will see what we can infer from the general characteristics of the event and from the evolving emission line concerning the coronal magnetic structure in the source region. We will conclude in Sect. 5.

2. Observations

2.1. General description and coronal configuration

An overview of the entire event is given in Fig. 1. It shows the dynamic spectrum recorded by *ARTEMIS*, and plotted on a contracted time scale over the full 100–500 MHz frequency range of the instrument. The event started around 1992 0217 0800 UT with a diffuse continuum emission band drifting from 300 to 150 MHz at a rate $df/dt \approx$ –0.1 MHz/s, slower than type II drift rates. No type II burst was recorded around 08 UT nor during the rest of the day, according to *Solar Geophysical Data* (SGD 572 I). Some local interferences are visible at 100–200 MHz around 09 UT in ARTEMIS spectrum (they are absent in *OSRA* and *IZMIRAN* spectra).

The radio continuum lasted until ≈ 1150 UT. Over basically its whole duration, it was modulated by a complex mixture of pulsations. Three main characteristic periods can be recognized: ≈ 3 min (Fig. 1), ≈ 10–20 s (Fig. 4), and ≈ 0.25 s (Fig. 7). Highly contrasted zebra patterns extended over an unusually large area of the time–frequency domain: ≈ 2 hours, 150–350 MHz. They revealed new sub-structures which we will describe in a specific section below. A unique "evolving emission line" added to the complexity of the event and will have its own section too.

At lower frequencies, a noise storm persisted during the entire event between 100 and 190 MHz. At higher frequencies, no significant microwave burst was observed. Only a small increase of 7 SFU above the quiet level was observed at 0847 UT by *IZMIRAN*'s 10 cm receiver. This event is entirely confined to metric and decimetric frequencies, with a sharp high-frequency cutoff that oscillates in the 350–480 MHz band.

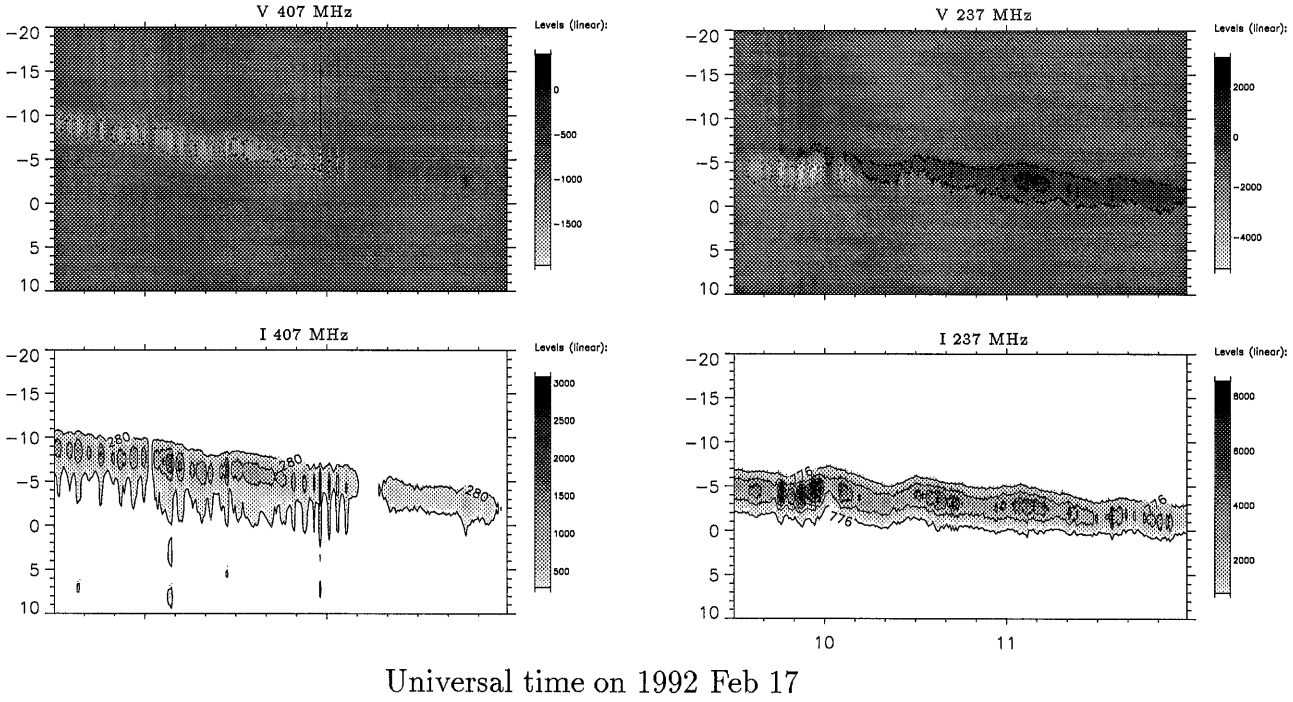

Fig. 2. Combined gray-scale and contour plots of the one-dimensional brightness distribution measured by NRH at two frequencies (237 and 407 MHz): intensity (Stokes I) and circular polarization (Stokes V). The vertical axes (channel number) give the coordinate along the terrestrial south-north direction (south is negative, 0 gives the center of the solar disk). The plotted fields have widths of about 5 $R_\odot$ at 237 MHz and 3 $R_\odot$ at 407 MHz. The motion of the source within the field of view is due to the rotation of the earth. Left-hand polarization is shaded black (solid contours), right-hand polarization white (dashed contours). The polarization reverses sign near 1005 UT at 237 MHz, and near 11 UT at 407 MHz.

The brightness distribution in the north-south direction and the circular polarization measured by *NRH* are plotted for 237 and 407 MHz, in a contracted time scale, in Fig. 2. Zebra stripes and pulsations (peaks at 237 MHz) are at the same position as the continuum during the entire event.

The polarization exhibits a very unusual behavior: it changes sign in the course of the event, both for the continuum and intensity peaks (caused by the fine structure). At 237 MHz, this reversal starts in the south-east part of the source at 1000 UT (Stokes V, transition from dashed contours to solid contours), and spreads gradually over to the north-west part by 1010 UT. By contrast, at 407 MHz the reversal takes place much later, around 1058 UT (just at the time of a new sub-structure in the zebra pattern at frequencies 200–265 MHz).

The corresponding 2-D radio source positions measured with *NRH* at its four frequencies are indicated in Fig. 3, superimposed on *Yohkoh/SXT* full-disk image. The cross in Fig. 3 gives the position and half-width of the radio source at 237 MHz; the positions at higher frequencies (327 and 407 MHz) are almost the same: the 407 MHz centroid is shifted merely by 0.035 solar radius to the south-west, while the 327 MHz centroid lies in between.

The radio source is located between active regions NOAA 7056 and 7058. The soft X-ray image reveals rather compact active region loops in NOAA 7058, which extend to very low altitude compared with the (projected) height of the radio source, while NOAA 7056 contains coronal structures on larger scales. Imaging observations by *Yohkoh/SXT* (Tsuneta 1991) show some variability of the brightest loop in NOAA 7058 during the orbit from 1045 UT to 1131 UT.

Three small H_α flares (SF C 4.1, 1N, SF C 3.6) were reported during the first half of this event between 08 and 10 UT, in active region NOAA 7058 (SGD 576 II); they were accompanied by three small X-rays enhancements (at wavelengths 1–8 Å), recorded by the GOES-7 soft X-ray detector (SGD 571 I). Also an active dark filament appeared in NOAA 7056 (S08 W39), after 1110 UT (SGD 576 II).

2.2. Slow pulsations

The 3-min pulsations persisted over the entire duration of the event, as clearly seen on Fig. 1. These pulsations have a sharp high-frequency cutoff at $\approx$ 400 MHz from 0920 to 1050 UT, drifting towards lower frequencies afterwards.

Irregular pulsations with varying periods of 10-20 s are also present during most of the event. They are especially noticeable on the time derivative of the flux density: bottom parts of *ARTEMIS* spectra on Fig. 4.

2.3. Zebra patterns

According to the *ARTEMIS* and *IZMIRAN* spectrographs, the first fibers oscillating in frequency, or zebra patterns, appeared at $\approx$ 0830 UT and continued until 1120 UT. Fig. 5 allows us

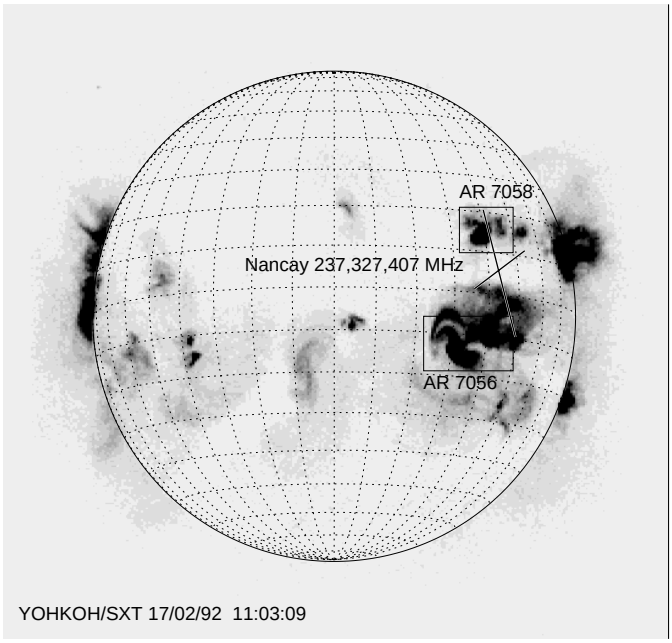

Fig. 3. Radio position and half width of radio source (cross) measured with *NRH* at 237 MHz (long bars), 327 and 407 MHz (short bars) around 11 UT, overlaid on a *Yohkoh/SXT* image recorded at 1103 09. UT (thin Al.1 filter, exposure 78 ms). Note that some small flares occurred in active region 7058 (N13 W40) between 08 and 10 UT.

to compare dynamic spectra recorded simultaneously by *OSRA* and *IZMIRAN*; zebra patterns exhibit a detailed correlation between these two distant observatories, proving their solar origin.

The zebra patterns evolve during the event from a non-stationary phase, with numerous sharp changes in the frequency drift-rate, to almost parallel lines (along the time axis) after 1037 UT.

For the first time, we can see an entire frequency range occupied by zebra patterns during almost 3 hours. Because of frequency gaps between neighboring channels of *ARTEMIS*, zebra patterns show up as white and black dots, especially in the time derivative of the dynamic spectra (bottom parts in Fig. 4). The low-frequency boundary of the zebra patterns is fairly stable at frequencies of $\approx$ 190 MHz, while the high-frequency cutoff oscillates between 250 and 350 MHz. In comparison, other zebra pattern events have been observed at much lower frequencies (e.g. down to 45–50 MHz: Bakunin et al. 1990).

Inspecting a typical time interval, e.g. around 1101 UT (Fig. 4), we observe n=8 zebra stripes over the frequency range from f_1=275 MHz to f_2=325 MHz in the *ARTEMIS* spectrum; we deduce the average frequency separation between zebra stripes $\Delta f = (f_2 - f_1)/(n-1)$=(325-275)/7 $\approx$ 7 MHz.

Both *IZMIRAN* and *OSRA* spectra show that the frequency separation may change irregularly with frequency. For instance, at 0951 36. UT (see arrows in Fig. 5), Δf keeps a nearly uniform value $\approx$ 5.6–6.0 MHz between 233 and 267 MHz. Later on, at 1039 40. UT, it varies irregularly between 6.0 and 8.5 MHz in the same frequency range. The same effect was mentioned by Slottje (1981).

Sometimes, Δf exhibits a systematic trend with time; for instance, from 1000 to 1100 UT, it increases from $\approx$ 5 to 8 MHz.

2.4. New features in the fine structure

Two new kinds of sub-structures are visible in the zebra patterns recorded by *IZMIRAN*.

The first new feature is a rapid frequency shift of the whole zebra pattern, like at 0958 21. UT (Fig. 6, upper panel). All zebra stripes jump by an amount comparable to the zebra stripe separation. They do not do it simultaneoulsy, but with a frequency drift rate $df/dt \approx$ –50 MHz/s, comparable to type III burst drift rates. The zebra pattern seems to be broken along a slanted "fault". These frequency shifts occur frequently and randomly during the whole event, without any characteristic time period, sometimes within a second, sometimes episodically during one minute.

The second new feature consists in sub-splitting of a zebra stripe into two separate stripes, like at 1058 21.–22. UT (Fig. 6, bottom panel, after the hook). The split stripes have different characteristics: the low-frequency stripe is continuous, while the high-frequency stripe consists of regular dots with a characteristic period $\approx$ 0.25 s. These frequency splittings last for minutes. Occasionally two continuous stripes exhibit chaotic frequency drifts, or cross each other.

2.5. Evolving emission line: EEL

Right along the high-frequency cut-off line of the pulsating continuum, and following its frequency fluctuations, a narrow band emission, 10–15 MHz wide, oscillates almost sinusoidally in frequency. We will hereafter refer to it as the EEL: *Evolving Emission Line*. These oscillations occur in phase with the flux density of broadband pulsations: cut-off/EEL frequency maxima (minima) correspond to flux maxima (minima). Fig. 4 shows this effect in detail. One or two weaker additional bands (15–20 MHz wide) appear episodically on the low frequency side of the EEL, at 20 to 100 MHz from it.

The EEL is distinctly different from zebra pattern stripes. It mostly consists of one single emission band instead of many, with a larger relative bandwidth $\Delta f/f \approx$ 12 MHz/450 MHz $\approx$ 0.03 (instead of $\approx$ 1.3/250 $\approx$ 0.005 for zebra stripes). It is also continuous over two hours instead of being intermittent.

Very dilated plots using *ARTEMIS* high time resolution (Fig. 7), reveal that the EEL is structured into a succession of dots every 0.25 s or so. Each dot consists of an emission (black) on its low-frequency side and an absorption (white) on its high-frequency side. The duration of each dot is about half their period, that is $\approx$ 0.12 s. Fig. 8 shows time profiles of the EEL on successive channels of *ARTEMIS*.

The position of the EEL could be measured when it straddled the *NRH* frequency 407 MHz, during the period 1058–1107 UT (Fig. 2, Stokes I). It is north of the continuum / zebra pattern common position, and its center is approximately at the same position as the main continuum at 237 MHz, as can be checked on the more detailed disk map of Fig. 3.

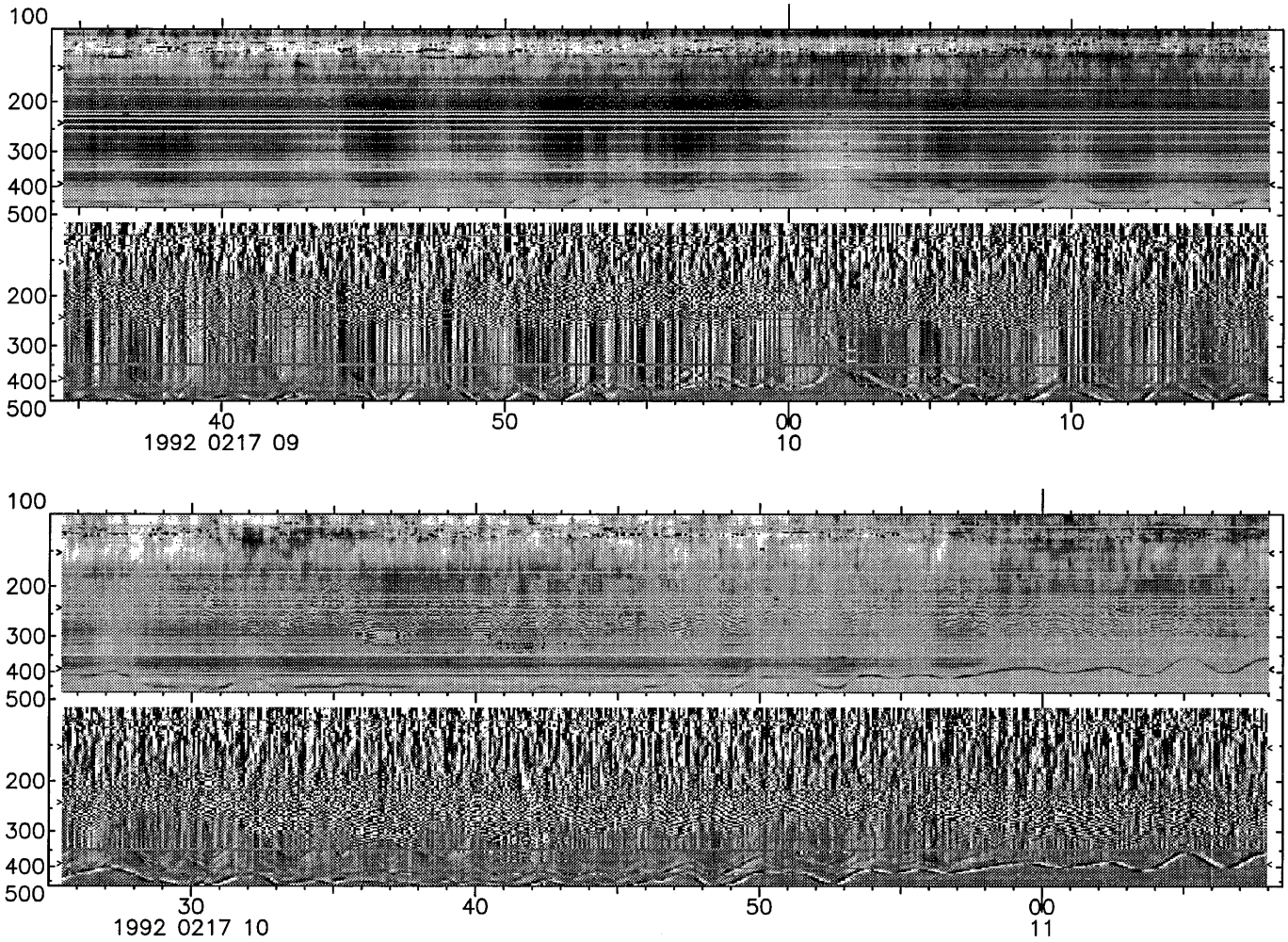

Fig. 4. *ARTEMIS* dynamic spectrum over a 1 h 45 min period (flux density / time derivative). Besides the 3 min pulsations (in phase with the EEL around 400 MHz), additional pulsations with periods of $\approx$ 20 s can be seen, as well as zebra patterns between 190 and 350 MHz, and noise storm at frequencies $<$ 190 MHz.

At variance with the continuum, the polarization of the EEL (six peaks between 1055 and 1106 UT) does not change: it stays right-handed (Stokes V $<$0) all the time.

2.6. Fast pulsations: sudden reductions

Fast pulsations show up on high time resolution plots such as in Fig. 7. They have a period of $\approx$ 0.25 s, similar to the period of bright dots making up the upper frequency component of split zebra stripes as well as the EEL.

These pulsations have a remarkably high frequency drift rate of $\approx$ –1000 MHz/s, consistent with the fact that the bright dots are nearly simultaneous between different zebra stripes. They turn out to be wide band "*sudden reductions*", with roughly the same low-frequency limit as the zebra patterns, i.e. $\approx$ 190 MHz.

Possibly rooted on them, diffuse, drifting structures appear at lower frequencies, with drift rates $df/dt \approx$ –50...–100 MHz/s similar to those of type III bursts (Fig. 7).

Fig. 8 shows that *sudden reductions* occur only where the background emission is enhanced relative to the quiet continuum.

3. Interpretation of the zebra pattern and its fine structure

3.1. General theories of type IV radio emission

It is generally believed that type IV radio burst fine structures are caused by particle injections into a magnetic trap and formation of a loss-cone distribution, giving rise to different plasma instabilities. The continuum emission of metric and decimetric type IV radio emission is usually connected with electrostatic loss-cone and Cherenkov instabilities of highgly energetic electrons, and their subsequent transformation into electromagnetic (transverse "t") waves (Stepanov 1973; Kuijpers 1975). "Sudden reductions" of coherent radio emission have been interpreted as due to fresh particle injections which fill up the loss-cone, thereby quenching the instabilities temporarily, until they

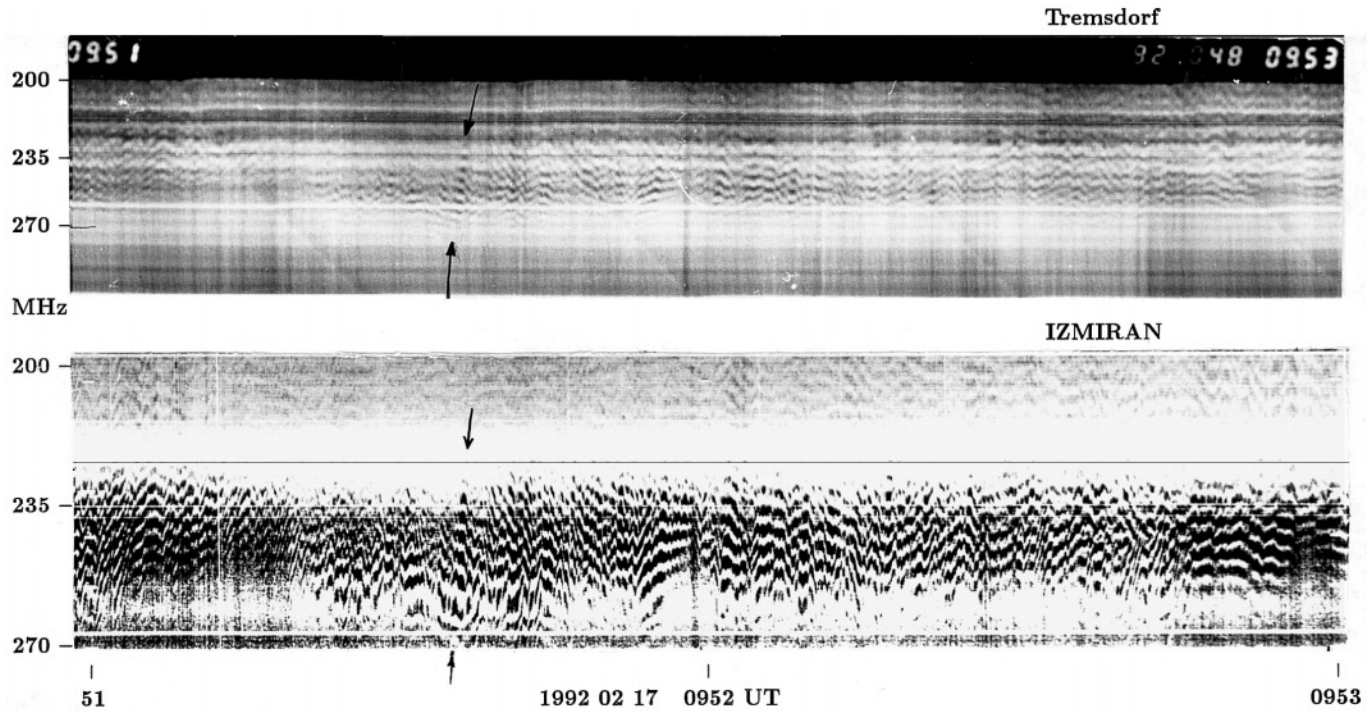

Fig. 5. Simultaneous dynamic spectra of zebra pattern from *OSRA* and *IZMIRAN* spectrographs on the same time scale. They exhibit numerous details in common. The arrows point to a particularly sharp frequency change of zebra stripes, occurring quite simultaneously. The good agreement between the spectra recorded at these two distant observatories is evidence for the solar origin of the structures observed.

precipitate again and restore the original loss-cone distribution (Zaitsev & Stepanov 1975; Benz & Kuijpers 1976).

Fiber bursts (or intermediate drift bursts) are generally explained by the non-linear coupling of Langmuir waves ("l") with whistler waves ("w"): $l + w \Rightarrow t$ (Kuijpers 1975; Chernov 1976b; Fomichev & Fainstein 1988), or alternatively in terms of strong whistler turbulence (Bernold & Treumann 1984; Mann et al. 1987; Treumann, Güdel & Benz 1990).

Zebra patterns are more complicated structures, with many different mechanisms proposed (Chiuderi et al. 1973; Zheleznyakov & Zlotnik, 1975 a,b,c; Fedorenko 1975; Kuijpers 1975, 1980; Berney & Benz 1978; Fomichev & Fainstein 1981; Mollwo 1983, 1988). The majority of these models are based on electrostatic emission at the double plasma resonance:

$$\omega_{UH} = (\omega_{Pe}^2 + \omega_{Be}^2)^{1/2} = s\omega_{Be} \quad (1)$$

with ω_{UH} = upper hybrid frequency, ω_{Pe} = electron plasma frequency, ω_{Be} = cyclotron frequency and s= integer harmonic number.

The most advanced model in this category, proposed by Winglee & Dulk (1986), is based on cyclotron non-saturated maser emission driven by a loss-cone electron distribution. However, several difficulties remain with all these versions:

– the frequency separation between zebra stripes Δf corresponds to the cyclotron frequency; this is hard to reconciliate with its often irregular variation with frequency;
– the magnetic field deduced from Δf, a few 10^{-4}T, seems too low for the active region corona;
– there is no explanation for zebra stripes on intense continuum in the presence of strong modulation (absorptions).

Hence a widely accepted theory of zebra pattern has not yet emerged. An important point missing in previous theories is that a loss-cone distribution generates whistlers which in turn affect the electron velocity distribution (Omura & Matsumoto 1987). In addition, many features of zebra stripes and fiber bursts are similar. This led Chernov (1976, 1989) to propose a common interpretation for these two kinds of fine structure, based on Langmuir wave and whistler coupling $l + w \Rightarrow t$.

We will now test these two leading theories given the new features observed in our type IV burst.

3.2. The Winglee & Dulk (1986) model

The electron cyclotron maser mechanism of Winglee & Dulk (1986) takes place at the cyclotron resonance:

$$\omega - k_\parallel v_\parallel - \frac{s\omega_{Be}}{\gamma} = 0 \quad (2)$$

($k_\parallel$, $v_\parallel$ = wave number and fast electrons velocity both parallel to the magnetic field, γ = Lorentz factor) under the conditions: $v_\parallel \ll v_\perp$, s - sufficiently high (10...20...), $k_\perp v_\perp \approx s\omega_{Be}$, and distribution function derivative $\partial F/\partial v_\perp > 0$.

Using characteristic values reported in Sect. 2.3 for our event, we find that the gyrofrequency, given by the zebra stripe separation, is $f_{Be} = \Delta f \approx 7$ MHz, and corresponds to a mag-

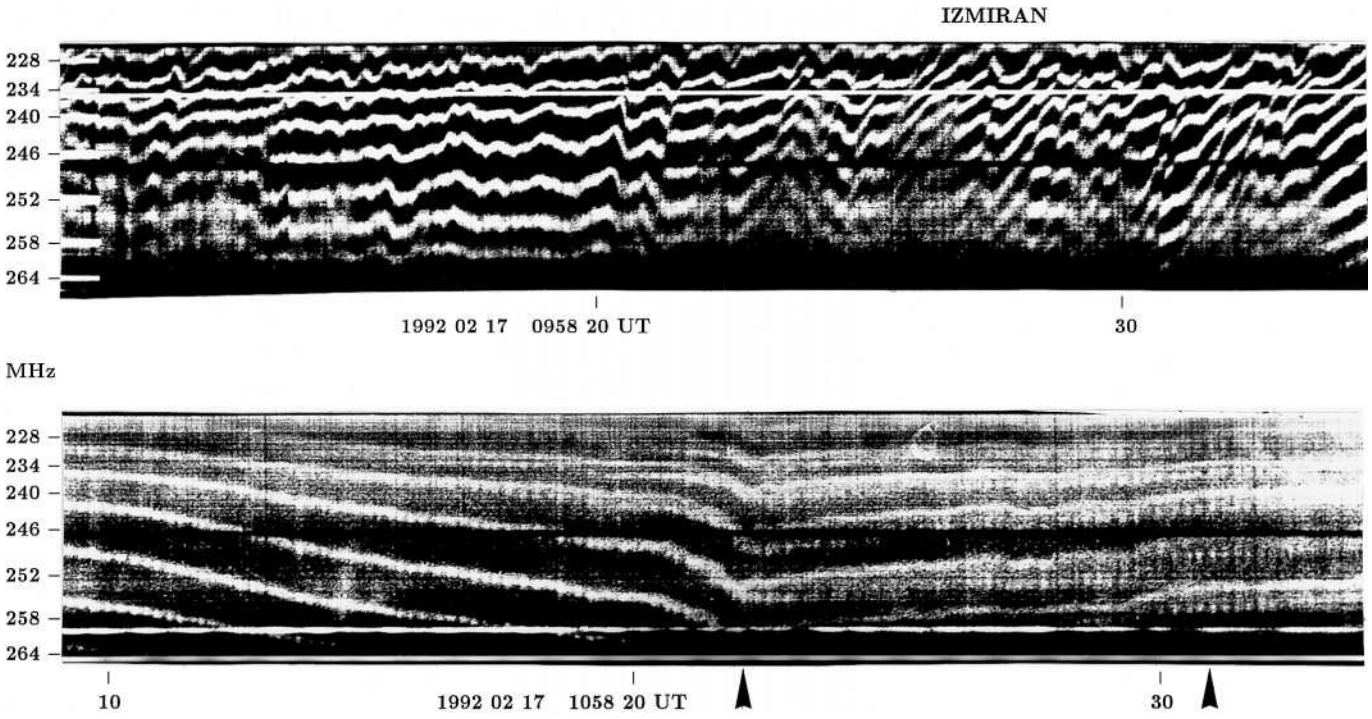

Fig. 6. Two enlargements of zebra patterns recorded with the *IZMIRAN* spectrograph with high resolution in the range 226–265 MHz, illustrating the two kinds of new sub-structures discovered. The top panel shows numerous sudden frequency shifts of zebra patterns. The bottom panel shows a few cases of stripe splitting (first arrow) and the dot-like structure of the upper-frequency component (second arrow).

netic field $B \approx 2.5 \times 10^{-4}$T. We also find harmonic numbers $s = f/f_{Be} \approx 39$ to 46. For such high values of s, we have:

$$\omega_{Pe} = \omega_{Be}\sqrt{s^2 - 1} \approx s\omega_{Be} = \omega_{UH} \ . \quad (3)$$

The plasma frequency corresponds closely to the upper hybrid frequency or observed frequency, from which we deduce the electron density in the zebra source: $n_e = 0.9 - 1.3 \times 10^{15}$ m^{-3}.

The resulting Alfvén velocity in the source is $v_A = 2.2 \times 10^{16} B/\sqrt{n_e} \approx 170 \times 10^3$ m/s and the plasma beta $\beta = (v_s/v_A)^2 \approx 1$. We are faced to the general difficulty with this kind of model: β is usually much smaller than 1 in the corona above active regions.

Let us note that the ratio of the plasma frequency to the gyrofrequency $\omega_{Pe}/\omega_{Be} \approx s \approx 40$ is rather high, but corresponds to a regime where growth of upper hybrid waves is still considered to be possible.

Zebra stripes wiggle by about 5 MHz on time scales of minutes, as shows the enlarged *IZMIRAN* spectrum in Fig. 6, top panel. According to Eq. (3), these frequency variations $\Delta\omega/\omega \approx 5$ MHz / 300 MHz ≈ 0.02 at s constant are produced either by electron density variations $\Delta n_e/n_e = 2\Delta\omega_{Pe}/\omega_{Pe} \approx 2\Delta\omega/\omega \approx 0.04$ or by magnetic field variations $\Delta B/B = \Delta\omega_{Be}/\omega_{Be} \approx 0.02$, or a combination of both. Such fluctuations are quite possible over a minute or so, for instance as a result of more or less chaotic MHD oscillations in a magnetic flux tube as we will discuss it in Sect. 4.2.

The plasma and gyro- frequencies ω_{Pe} and ω_{Be} may present spatial fluctuations too, e.g. as a result of longitudinal oscillations, likely to accompany radial oscillations. Then Eqs. (1) and (2) may be verified in several places along the loop, leading to broadening and even bifurcation of individual zebra stripes into two or more components. This could account for the observation of split stripes, but does not explain why we observe no more than 2 components.

Loop oscillations can also modulate the electron distribution at the mirror points, affecting the growth rate of coherent upper-hybrid waves driven by the loss-cone instability. Because of the large amplification factors involved, this will result in a rapid sequence of switch on/off emissions, as described in the *sudden reduction model* of Benz & Kuijpers (1976). Such rapidly fluctuating processes may be responsible for the observed dot-like emission features on time scales of 0.25 s in the fine structure of individual zebra stripes.

However, slow modulations of the magnetic loop, propagating at the Alfvén speed v_A, might not be able to modulate the loss-cone instability fast enough. An alternate interpretation of the 0.25 s structures is that they are due to new injections of fast particles (Zaitsev & Stepanov 1975; Benz & Kuijpers 1976). The simultaneity of bright dots in the EEL and split zebra stripes (very broadband sudden reductions on Fig. 7) seems to require such fast particle beams. Frequency shifts of zebra stripes, with type III-like drift rates, could also be the result of such sharp changes of $v_\perp$.

But then another problem arises: if $v_\parallel$ increases, both conditions $v_\parallel \ll v_\perp$ and $\partial F/\partial v_\perp > 0$ would break down and the instability would switch off!

Whatever the alternative, several other challenges face the Winglee & Dulk model:

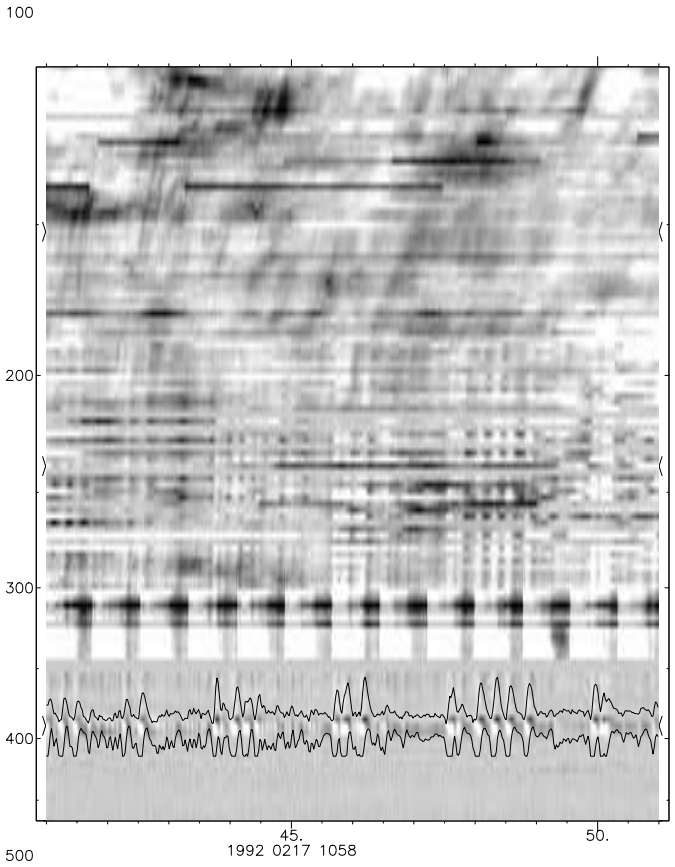

Fig. 7. *ARTEMIS* flux density spectrum at high time resolution, over a time interval when zebra patterns exhibited marked sub-structures. Zebra stripes are the horizontal black bands around 250 MHz; each one is visible in a given frequency channel for a few seconds only, because of its frequency drift. The EEL is visible on 2 channels around 400 MHz; we superimposed the 2 corresponding time profiles showing the 0.25s period clearly. This set-up emphasizes the spectral structure of the EEL, made up of emission (black) and absorption (white) dots, synchronized with zebra stripe dots and 0.25 s sudden reductions. At frequencies <200 MHz, we notice fast structures drifting at type III rates.

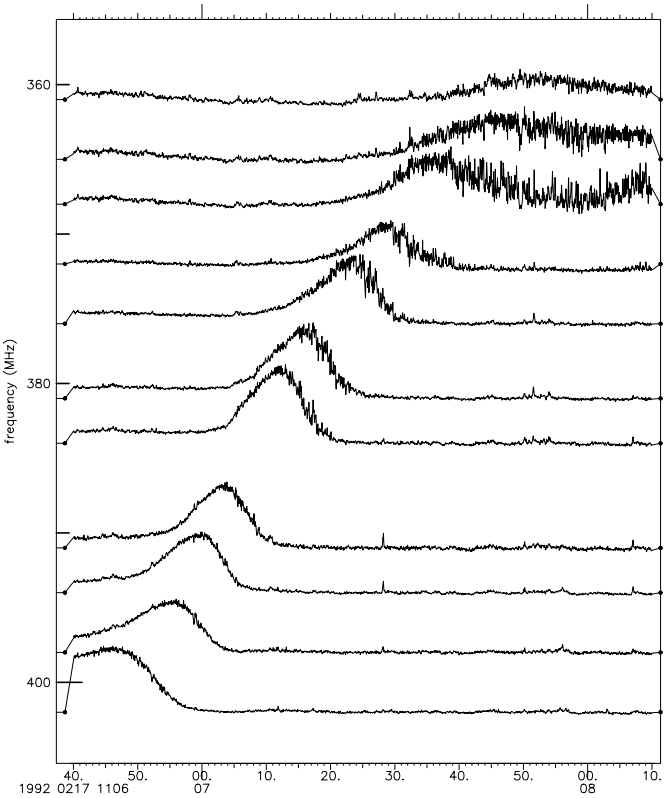

Fig. 8. Time profiles on *ARTEMIS* high frequency channels during a 1 min 30 s period. The EEL moves from the 402 MHz channel to the 361 MHz channel. The ≈ 0.25 s sudden reductions (fast pulsations) are mostly visible when the EEL reaches its minimum frequencies. We note also that the background is at a higher level on the low frequency side of the EEL.

a) why do we never observe more then 2 components in split stripes?
b) why only the upper-frequency components of split stripes after 1058 UT have the dot-like structure?
c) why does stripe splitting happen during some minutes only at the end of the event, while the pulsations show that loop modulations last for 3 hours?

3.3. The $l + w \Rightarrow t$ model

In connection with the above mentioned difficulties, we will try now to interpret the various features of our event within the $l + w \Rightarrow t$ model (Chernov 1976b, 1989).

A system of standing whistler waves w is driven by a loss-cone electron distribution of fast electrons in the entire magnetic trap at the cyclotron resonance:

$$\omega_w - k_\parallel v_\parallel - s\omega_{Be} = 0 \tag{4}$$

with s=+1 (normal Doppler effect) or s=–1 (anomalous Doppler effect) depending on the form of the distribution function (Maltseva & Chernov 1989).

As in the other models, this quasi-linear wave–particle interaction leads to quenching the loss-cone instability at more or less regular time intervals of the order of the whistler growth rate $\geq 0.2s$ (Kuijpers 1975, p.59).

The coupling of discrete whistler wave packets with Langmuir waves l generates electromagnetic waves t with the conservation laws:

$$\omega_w + \omega_l = \omega_t \qquad k_w + k_l = k_t \tag{5}$$

where k_w = whistler wave number ≈ 2 m^{-1} (Kuijpers 1975; Fomichev & Fainstein 1988; Chernov 1990).

As maximum whistler amplification is localized in narrow zones of characteristic size $l_w \approx 10^3$km, the process results in drifting emission/extinction bands, which will show up as fiber bursts or zebra pattern, depending on duct or oblique whistler propagation (Chernov 1976b, 1990; Maltseva & Chernov 1989).

The plasma density in the source is given by $\omega_{Pe} \approx$ observing frequency ω, like in the Winglee & Dulk model, that is again $n_e \approx 10^{15}$ m^{-3}. But a major difference in the present model is that the magnetic field strength B is related to the frequency separation between the emission and the neighboring low frequency absorption of a zebra stripe by $\Delta f_{ea} \approx 0.1 \times f_{Be}$ (Chernov 1990). In our event, $\Delta f_{ea} \approx \Delta f/2 \approx 3$ MHz at a frequency ≈ 250 MHz gives: $B \approx 11 \times 10^{-4}$ T, $\omega_{Pe}/\omega_{Be} \approx 8$, $v_A \approx 800 \times 10^3$ m/s and $\beta \approx 0.05$. The latter value for the plasma beta is smaller and more plausible than in the previous model.

When a new beam of particles is injected (new $v_\parallel$), ω_w changes suddenly according to Eq. (4), and conservation Eqs. (5) break down locally, but are quickly restored at nearby plasma levels with a different value of ω_l. This will result in a sudden shift of the frequency ω_t, propagating from one zebra stripe to the next one at the speed of the beam. This corresponds precisely to the observed "frequency shifts" (Fig. 6, top panel) at drift rates similar to type III bursts.

Another consequence of the injection of a new beam is that the velocity distribution is suddenly filled up with high velocities parallel to the magnetic field, which tend to turn on the instability on the anomalous Doppler resonance (Gendrin 1981). This offers a natural explanation for the split zebra stripes as due to simultaneous whistler instability at normal Doppler resonance $\omega_{w,s=1} = k_\parallel v_\parallel + \omega_{Be}$ and at anomalous Doppler resonance $\omega_{w,s=-1} = k_\parallel v_\parallel - \omega_{Be}$ at slightly different plasma levels. For $(\omega_{w,s=1} - \omega_{w,s=-1})/2\pi \approx 2$ MHz we need $v_{\parallel,s=1} \approx 16 \times 10^6$ m/s and $v_{\parallel,s=-1} \approx 26 \times 10^6$ m/s, which are quite possible velocities in the source.

Additional beams with a narrow velocity dispersion (high $v_\parallel$) do not change the conditions of instability for the normal Doppler effect (high $v_\perp$). Therefore, only the high frequency component of a split zebra stripe will be structured by these beams into a succession of emission dots, in synchronization with sudden reductions.

The $l + w \Rightarrow t$ model thus nicely accounts for the characteristic features of zebra stripe frequency shifts and splittings, and for their occurrence at times of enhanced sudden reductions, that is in the midst of repeated injections of electron beams with high $v_\parallel$.

4. Discussion: magnetic structure and energetic particles

4.1. Reconnection in trans-equatorial loop

Unlike flare-related type IV bursts, the 1992 0217 type IV occurred without any major activity in the chromosphere and low corona. It thereby resembles other events displaying the same fine structure (cf. Slottje 1981, Chernov et al. 1994). We infer that the event mainly reveals processes in the middle and upper corona, likely to be connected to large-scale magnetic reconfiguration, as it may occur, e.g., during the restoration of magnetic structures after a coronal mass ejection (CME).

Looking at Fig. 3, it is tempting to locate the source within a large trans-equatorial closed loop structure connecting AR 7056 and AR 7058, comparable to other large scale loops sometimes connecting different active regions as traced from radio type U-bursts simultaneously observed with *NRH* and *Yohkoh/SXT* (Aurass & Klein 1997). A trans-equatorial connection between the two active regions is supported by the appearance of a streamer-like structure above the two regions, visible at the limb from *Yohkoh/SXT* and Mauna-Loa Mk3 observations 1–3 days later.

The remarkable feature of polarization reversal in the course of this type IV burst may be due to a modification in the large-scale magnetic configuration. The variation with time of the frequency separation between zebra stripes does show that the magnetic field in the source varies. The polarization reversed at 237 MHz just at the same time an active dark filament appeared in the southern part of the active region, suggesting magnetic reconnection high in the corona (cf. Fig. 1 in Steele and Priest 1989).

However the polarization reversal could also result from the interplay between two parts of the source with opposite polarizations. At 407 MHz the polarization reversed just when the EEL crossed this frequency, without any conspicuous change of the source position. This would suggest that emission at frequencies below and above the EEL come from opposite sides of the current sheet.

4.2. Magnetic arch oscillations

The nature of radio pulsations with different time scales is usually divided into three groups (Aschwanden 1987): 1) magneto-hydrodynamic (MHD) flux tube oscillations, where the emissivity of trapped particles is modulated by a standing or propagating MHD wave, 2) cyclic self-organizing systems of plasma instabilities (wave-particle or wave-wave interactions), and 3) modulation of the particle acceleration process.

Pulsations with periods of about 3 min (and also superimposed shorter periods of 15–20 s) were observed throughout the whole 4 hour duration of the event. After 1058 UT, when the sense of circular polarization changed, the pulsations started decaying (Fig. 4). Before that time, a magnetic loop appears to oscillate continuously with a period of ≈ 3 min.

A disturbance at one footpoint of the loop can generate oscillations in the "kink" or in the "sausage" mode. As the loop is denser than the surrounding medium, the Alfvén speed presents a minimum there and MHD waves tend to be trapped inside the loop. A standing mode of fast magnetoacoustic waves will build up with a time period of (Roberts et al. 1984):

$$\tau_f \approx \frac{2L}{j v_{Am}} \tag{6}$$

where L is the length of the loop, j is the number of nodes in the loop, and v_{Am} the mean Alfvén speed. The slowest pulsations observed have a mean period τ_f=180 s and correspond probably to the fundamental mode j=1.

Using the Alfvén speed determined in the Winglee & Dulk model, we deduce $L = \tau_f v_A/2 \approx 180 \times 170 \times 10^3/2 \approx 15 \times 10^6$m. This is the size of a flaring loop, not of a trans-equatorial, high-corona loop. And the magnetic field in such a small loop

would be much larger than the 2.5×10^{-4}T determined in this model.

In the $l+w \Rightarrow t$ model, we deduce $L \approx 180 \times 800 \times 10^3/2 \approx 70 \times 10^6$m. This is about the minimum length we expect for a trans-equatorial loop connecting two active regions. Let us note that L would actually be j times as large for higher oscillation harmonics. The magnetic field estimated in this model, $B \approx 11 \times 10^{-4}$T, is quite compatible with the coronal height reached by such a loop.

Alternatively, slow mode oscillations, which propagate essentially with the sound speed, would yield similar periods for a smaller loop (Roberts et al. 1984); this does not seem to be the case here.

The faster pulsations, with a mean period $\approx$ 15–20 s, might correspond to a higher mode of oscillations $j \approx 10$. But as they started to decay at the same time the polarization at 237 MHz changed sign ($\approx$ 1014 UT), they might also have involved a smaller loop at the beginning of the event.

While the density and magnetic field do not change on the first order for the kink mode (oscillations with constant cross-section), they change reciprocally with the loop cross-section for the sausage mode (particle number and magnetic flux conservation). That is, in the limit of small amplitudes, $\Delta n_e/n_e = \Delta B/B = 2\Delta r/r$. Thus fluctuations of the loop radius by only 1% will produce the 2% fluctuations of the magnetic field required to account for the frequency wiggling of zebra stripes (Sect. 3.2). Assuming B constant, the radius would have to fluctuate by 2% to produce the required 4% fluctuations in density.

The observed frequency fluctuations, however, are not strictly periodic (see Fig. 6), as expected for a global MHD oscillation mode. Impulsively generated MHD waves (Roberts et al. 1984), which have a more chaotic and less regular time evolution, are perhaps more appropriate to describe the observed time variability of zebra patterns.

4.3. EEL and current sheet

The EEL around 400 MHz has to be produced by a coherent emission mechanism, because incoherent (free-free or gyrosynchrotron) emission would produce much broader spectra. The EEL being at the highest frequency emitted, it is tempting to locate its source in the densest part of the whole radiating volume, that is inside the current sheet where magnetic reconnection proceeds. This may also account for its small bandwidth.

The EEL consists of emission and absorption dots (Figs. 7 and 8) occurring just between the $\approx$ 0.25 s sudden reductions which affect the whole frequency range of the event. As sudden reductions result from the quenching of the loss-cone instability by new injections of fast particles inside the current sheet, the EEL is likely due to a coherent electron-cyclotron maser emission of the loss-cone instability (Winglee & Dulk 1986) at the upper hybrid frequency at double plasma resonance. However, we still have to understand the particular emission/absorption spectrum of individual dots making up the EEL.

The disappearance of the EEL during the minima of the 3 min pulsations may be due to the breakdown of the double plasma resonance, as the magnetic field is minimum at these times (kink or sausage mode).

Let us see what we can learn from the episodic occurrence of 2 or 3 harmonics (e.g. Fig. 4, between 1024 and 1040 UT). The regime $\omega_{Pe}/\omega_{Be} < 1$, with an electromagnetic magneto-ionic mode at the fundamental gyro-level, would require a magnetic field $B > 140 \times 10^{-4}$T (at a plasma frequency of 400 MHz). From the zebra pattern we deduced much smaller values, B= 2.5 or 11 $\times 10^{-4}$T. As a consequence, the EEL source would have to be at much lower altitude than the zebra source, typically in the loss-cone region near the footpoints of the arch. However, the EEL at 407 MHz is observed almost at the same position as the continuum at 237 MHz (see *NRH* observations in Fig. 2).

We conclude that the EEL is more likely produced in the regime $\omega_{Pe}/\omega_{Be} > 1$, where gyro-resonant wave growth usually contributes to multiple harmonic bands, such as in the case of upper hybrid waves. Simultaneous cyclotron harmonics are produced when the double plasma resonance is fulfilled at some levels during enhancements of the magnetic field (maxima of the 3 min pulsations).

The frequency separation between such harmonics varies between $\approx$ 50 and 80 MHz, which corresponds to a maximum magnetic field strength in the source $B \approx$ 17–28 $\times 10^{-4}$T, consistent with the 11×10^{-4}T deduced from the $l + w \Rightarrow t$ model for zebra patterns at a lower frequency (250 MHz) where we do expect a weaker field.

We can also conceive that the EEL frequency will oscillate roughly in phase with the pulsations of the continuum source.

5. Conclusion

We have described the unusually complex radio event of 1992 0217, which, for more than 2 hours, exhibited a wealth of fine structures, some of them seen for the first time: various periodicities ranging from 0.2 s to 3 min, polarization reversal, very long-lasting oscillating zebra patterns, many sudden global frequency shifts, splitting and dot-like structure of individual zebra stripes, evolving emission line (EEL)...

Interpreting zebra patterns with the (loss-cone driven) electron cyclotron maser emission theory, operating at upper-hybrid frequency at the double plasma resonance, would give an average density of $n_e = 10^{15}$ m^{-3} and a magnetic field of $B = 2.5 \times 10^{-4}$ T. Oscillations of a large magnetic loop in the sausage mode with an amplitude of 1 or 2% are sufficient to produce the temporal frequency oscillations and the band splitting of zebra patterns. But this model requires too low a magnetic field (plasma beta $\beta \approx 1$), and does not readily explain the characteristics of split stripes: at most two components and a dot-like structure for the upper-frequency component only.

These features are more readily explained with the second model, $l + w \Rightarrow t$: whistler loss-cone instability simultaneously at normal and anomalous Doppler cyclotron resonances, corresponding to the 2 components of split stripes. Periodic injections of new particles account for the fast pulsations (sudden reduc-

tions). This model gives an acceptable value for the plasma beta in the upper corona ($\beta < 1$).

On the other hand, the electrostatic maser at double plasma resonance explains the characteristics of the EEL well, in its frequency range of 350–450 MHz. (The electromagnetic maser would require too high a magnetic field.) Yet, the unique occurrence of the EEL in this event remains puzzling, and the detection of the same kind of isolated emission line in other type IV bursts would be most valuable.

Acknowledgements. G.C. is grateful for the support by Paris Observatory that enabled him to work with colleagues at Meudon, by the Russian Foundation of Basic Research, grant No.96-02-17024a, and by the Federal Astronomy Program. The ARTEMIS radio spectrograph was funded by INSU (CNRS). The Nançay Radio Observatory is funded by the French Ministry of Education, the CNRS and the Région Centre. The *Yohkoh* data used in this paper were provided by the *Yohkoh* mission of ISAS, Japan, which was prepared and is operated by the international collaboration of Japanese, US, and UK scientists under the support of ISAS, NASA, and PPARC, respectively. We acknowledge D. Maia's help with the figures.

References

Aschwanden M.J., 1987, Solar Phys. 111, 113
Aurass H., Klein K.L., 1997, Astron. Astrophys. Suppl. Ser. 123, 279
Bakunin, 1990, Solar Phys. 135, 107
Benz A.O., Kuijpers J., 1976, Solar Phys. 46, 275
Berney M., Benz A.O., 1978, Astron. Astrophys. 65, 369
Bernold T.E.X., Treumann R.A., 1984, Astrophys.J. 264, 677
Chernov G.P., 1976a, Soviet Astron. 20, 449
Chernov G.P., 1976b, Soviet Astron. 20, 582
Chernov G.P., 1976c, Soviet Astron. 20, 589
Chernov G.P., 1989, Soviet Astron. 33, 649
Chernov G.P., 1990, Soviet Astron. 34, 66
Chernov G.P., 1996, Pisma v Astron. Journal, (in press)
Chernov G.P., Klein K.-L., Zlobec P., Aurass H., 1994, Solar Phys. 155, 373
Chernov G.P., Korolev O.S., Markeev A.K., 1975, Solar Phys. 44, 435
Chiuderi C., Giachetti R., Rosenberg H., 1973, Solar Phys. 33, 225
Fedorenkko V.N., 1975, Soviet Astron. (Astronomicheski J.) 52, 978
Fomichev V.V., Fainshtein S.M., 1981, Solar Phys. 71, 385
Fomichev V.V., Fainshtein S.M., 1988, Soviet Astron. (Astronomicheski J.) 66, 1058
Gendrin R., 1981, Reviews of Geophys. and Space Phys. 19, 171
Mann G., Aurass H., Voigt W., Paschke J., 1992, ESA Journal SP-348, 129
Kuijpers J., 1975, Collective Wave-Particle Interaction in Solar Type IV radio sources, Thesis, Utrecht
Kujpers J., 1980, in Radio Physics of the Sun, Kundu M.R., Gergely T.E.(eds), IAU Symp. No.86. 341
Maltseva O.A., Chernov G.P., 1989, Kinematika i Fizika Nebesnykh Tel 5, 39
Mann G., Karlicky M., Motschmann U., 1987, Solar Phys. 110, 381
Maroulis D., Dumas G., Bougeret J.L., Caroubalos C., Poquerusse M., 1993, Solar Phys. 147, 359
Mollwo L., 1983, Solar Phys. 83, 305
Mollwo L., 1988, Solar Phys. 116, 323
Omura Y., Matsumoto M., 1987, J. of Geophys. Res. 92, 8649 1994, in proc. of Kofu Symposium, NRO Report No. 360, p.263
Radioheliograph group, 1989, Solar Phys. 120, 193
Roberts B., Edwin P.M., Benz A.O., 1984, Astrophys. J. 279, 857
Slottje C., 1981, Atlas of fine structures of dynamic spectra of solar type IV-dm and some type II radio bursts, Utrecht Observatory
Stepanov A.V., 1974, Soviet Astron. 17, 781 (Original: 1973, Astronomichesky J. 50, 1243)
Treumann R.A., Güdel M., Benz A.O., 1990, Astron. Astrophys. 236, 242
Tsuneta S., 1991, Solar Phys. 136, 37
Winglee R.M., Dulk G.A., 1986, ApJ 307, 808
Zaitsev V.V., Stepanov A.V., 1976, Astron. Astrophys. 40, 135
Zheleznaykov V.V., Zlotnik E.Ya., 1975, Solar Phys. a) 43, 431, b) 44, 447, c) 44, 461